ACCURACY AND RADIOMETRIC STUDY ON LATEST GENERATION LARGE FORMAT DIGITAL FRAME CAMERAS

Ricardo Passini(*), Karsten Jacobsen(**), David Day(***)
(*)BAE SYSTEMS GP&S,ricardo.passini@baesystems.com
(**)Leibniz University Hannover, jacobsen@ipi.uni-hannover.de
(***)Keystone Aerial Surveys, dday@kasurveys.com

ABSTRACT: The latest generation large format digital frame cameras (the Z/I DMCII 140, 230 and 250 and the Microsoft UltraCam Eagle) have been used in large calibration test areas with the purpose of studying their geometrical accuracy performance as well as the radiometric characteristics of the rendered images. For this purpose, the cameras have been flown over large calibration test areas at different flying heights, forward and reverse flight patterns over the same flight line, and different overlaps (end and lateral). Both calibration test sites include a large quantity of control and independent check points used during adjustment and quality control. Several patterns of control point amounts and distributions were tested. All bundle block adjustments were carried out with self-calibration using specifically derived additional parameters for each camera with the purpose of removing possible systematic effects. In relation to the radiometric characteristics, several linear features evenly distributed over the entire area were cross sectioned along edges and their pixel grey shade studied through point spread functions that allow for the derivation of the effective dimension of the ground sample distance. This provides indirect data about the possible loss of information with respect to the theoretical value of the projected pixel size of each camera.

1. INTRODUCTION:

Digital aerial cameras have replaced analog cameras for most applications. The advantage of the digital cameras is obvious – the image quality of original digital images is higher and the difficultly and expensive of film processing is eliminated. As well, the scanning of analog images introduces some loss of information. The capacity of the large format digital aerial cameras has recently been extended. Z/I Imaging introduced very large monolithic CCD-array that does not requiring stitching of sub-images. Microsoft has developed a camera with a reduced pixel size which also leads to a larger number of pixels.

Camera	Number of pixels (camera)		Pixel size [µm]	f [mm]	Δt [sec]	Image size [mm]		Field of view in base	Mega-pixel
	x	y				x	y		
DMC	7680	13824	12.0	120	2	49.15	86.02	25.7°	106
DMCII 140	11200	12096	7.2	92	2	80.64	87.09	52.6°	135
DMCII 230	14144	15556	5.6	92	1.7	79.21	87.11	51.8°	220
DMCII 250	14656	17216	5.6	112	2.3	82.41	96.41	40.4°	249
UC D	7500	11500	9.0	101.4	1	67.50	105.5	36.8°	86
UC X	9420	14430	7.2	100.5	1.4	67.82	103.9	37.3°	136
UC Xp	11310	17310	6.0	100	2	67.86	103.9	37.5°	196
UC Eagle	13080	20010	5.2	80 / 210	1.8	68.02	104.1	46.1° / 18.4°	261

Table 1: Technical data of the various DMC and UltraCam large format versions

2. THE MICROSOFT ULTRACAM EAGLE TEST:

Organized by Keystone Aerial Surveys (KAS) and with the collaboration of staff members of BAE SYSTEMS GP&S, the UltraCam Eagle (UCE), recently acquired by KAS, was tested and photogrammetrically calibrated by using boresight data located in the regions surrounding the Northeast Philadelphia airport. The field area covers an area of approximately 38.5 Km^2. It includes two large shopping malls with very large parking lots with a wealth of painted parking lines. Crossed parking stripes and road markings that were recently painted in the pavement, were used as control points. This test area was covered by two flights at two different altitudes and crossing flight lines. Table 1 shows the geometrical details of the flight:

	End lap	Lat. overlap	Height (m)	GSD (cm)	# GCPs	# images
Low Altitude	60	60	780	5	84	200
High Altitude	60	60	2340	15	84	28

Table 2: Geometric parameters of the Eagle test field

Ground control points (GCPs) (84) were measured using GPS (RTK) procedure with a standard deviation of ±2 cm. Figure 2 shows a typical ground control point being observed and Figure 1 details of the control layout and regions of footprint overlap.

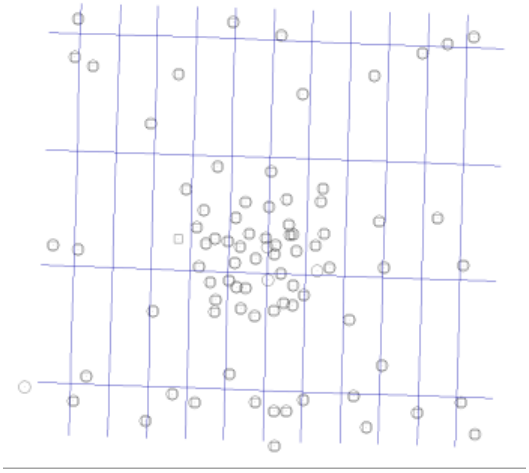

Figure 1a: Flight lines, GCPs and check points of the UCE flight

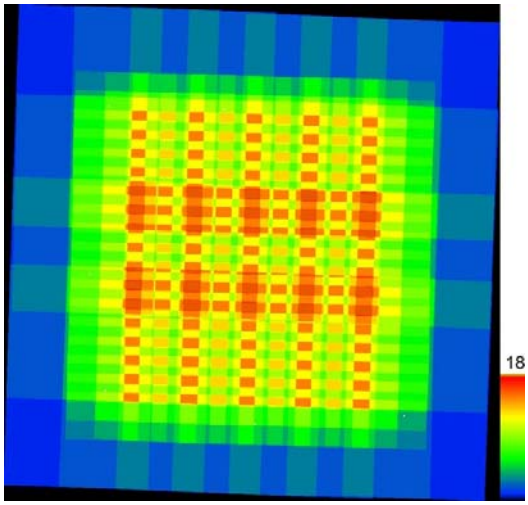

Figure 1b: Color coded image overlay of the UCE with up to 18 images per object point

INPHO's Match-AT was the tool used for the measurement of the GCPs. The manual collection of GCPs and the automatic determination of tie points were performed using the imagery from both flight heights. Tie points were created in an automatic matching environment where no manual tie points were created. The resulting block consisted of 5300 tie points that represent more than 25,000 image points.

Figure 2: Detail of GCP

The bundle block adjustment was attempted with multiple block configurations (i.e., only lowest flight, only the high flight, both simultaneous flight in one block adjustment, without and with self- calibration, different amounts and patterns of GCPs). In each case, where GCPs were removed to allow for different amounts and patterns of GCPs, those removed were used as Check Points (CHKs). As such the following cases were studied: I: 84 GCPs only; II: 45 GCPs and 40 CHKs; III: 28 GCPs and 56 CHKs; IV: 10 GCPs and 71 CHKs; V: 5 GCPs and 79 CHKs

2.1 SELF CALIBRATION:

Systematic image errors or, more precisely, the difference between the mathematical model of perspective geometry and the real image geometry, can be determined and respected with additional parameters in the bundle block adjustment. Different sets of additional parameters are in use and lead to satisfying results for analogue and digital images. The additional parameters may be based on a pure mathematical solution or physical justification. Ebner (1976) developed a set of additional parameters, able to compensate for the systematic image errors in the 9 von Gruber points of a photo (regular grid of 3 x 3 points). This mathematical justified set of parameters was extended by Grün (1979) to a set able to compensate for the systematic errors in a regular grid of 5 x 5 image points. Jacobsen (1980) used in the Hannover program system BLUH physical justified parameters, supported by some mathematical justification (table 3).

x, y = image coordinates normalized to maximal radial distance 162.6mm (scale factor: 162.6 / maximal radial distance) $r^2 = x^2 + y^2$ b = arctan (y/x)		
1. x' = x - y•P1	y' = y - x•P1	angular affinity
2. x' = x - x•P2	y' = y + y•P2	affinity
3. x' = x - x•cos 2b • P3	y' = y - y•cos 2b • P3	
4. x' = x - x•sin 2b • P4	y' = y - y•sin 2b • P4	
5. x' = x - x•cos b • P5	y' = y - y•cos b • P5	
6. x' = x - x•sinb • P6	y' = y - y•sin b • P6	
7. x' = x + y•r•cos b • P7	y' = y - x•r•cos b • P7	tangential distortion 1
8. x' = x + y•r•sin b • P8	y' = y - x•r•sin b • P8	tangential distortion 2
9. x' = x - x•(r^2-16384) •P9	y' = y - y•(r^2 - 16384) •P9	radial symmetric r^3
10. x ' = x - x•sin(r • 0.049087) • P10	y' = y - y•sin(r • 0.049087) • P10	radial symmetric
11. x' = x - x•sin(r • 0.098174) • P11	y' = y - y*sin(r •0 0.098174) • P11	radial symmetric
12. x' = x - x•sin 4b • P12	y' = y - y• sin 4b •P12	

Table 3: General additional parameters in Hannover program system BLUH

Moreover, the BLUH system package includes additional parameters specific for the Z/I DMC and the UltraCam camera series as well as for digital cameras having problems with the flatness of the CCD. They are included in table 4.

29. – 33 special parameters for the internal transformation of DMC sub-images			
34. x' = x – x*y*P34	y' = y	for upper right quarter	DMC Y 1
35. x' = x	y' = y – x*y*P35	for upper right quarter	DMC X 1
36. x' = x – x*y*P36	y' = y	for lower right quarter	DMC Y 2
37. x' = x	y' = y – x*y*P37	for lower right quarter	DMC X 2
38. x' = x – x*y*P38	y' = y	for lower left quarter	DMC Y 3
39. x' = x	y' = y – x*y*P39	for lower left quarter	DMC X 3
40. x' = x – x*y*P40	y' = y	for upper left quarter	DMC Y 4
41. x' = x	y' = y – x*y*P41	for upper left quarter	DMC X 4
42 – 49 scale parameters for UltraCam			
50 – 57 shift X parameters for UltraCam			
58 – 65 shift Y parameters for UltraCam			
66 – 73 UltraCam master images perspective			
79 common perspective deformation of DMC sub-images			
80 common radial symmetric parameter for DMC sub-images			
81-88 parameters for geometry at the corners of the image (problem of CCD flatness)			

Table 4: Special additional parameters in Hannover program system BLUH

2.2 EXPERIMENTAL RESULTS: The UltraCam Eagle: The image geometry of digital cameras can be analyzed by bundle block adjustment with self-calibration. With the additional parameters the systematic image errors – the difference between perspective geometry and the existing image geometry – can be determined. In addition, the image coordinate residuals of a bundle block adjustment can be analyzed for systematic image errors unaccounted for, by overlaying all image coordinate residuals according to their image position and averaging the residuals in image sub-areas.

No statistically significant difference in the systematic image errors for both flying heights could be seen, thus justifying the common handling of all images. The bundle block adjustment was made with the Hannover program system BLUH including a set of 12 additional parameters for standard application, a special set of parameters for the handling of the stitching of the sub-images (parameters 42 – 73) and special additional parameters for solving geometric problems at the image corners, often seen with digital cameras, the parameters 81 – 88 (Jacobsen et al 2010). As mentioned above the carried out experiments are shown in following table and graphical representation:

Tables 5, 6 and 7 show the bundle block adjustment results of the double coverage block (Two simultaneously adjusted flights), the results of the low altitude flight block (GSD=5 cm) and the results of the high altitude flight block (GSD=15 cm).

Block: Low + High Altitude Flight (GSD= 5cm respectively 15cm)							
additional parameters	σ_o µm	RMSE 84 GCPs [m]			MAX Errors 84 GCPs [m]		
		RMX	RMY	RMZ	M-X	M-Y	M-Z
no selfcalibr.	1.28	.023	.028	.030	.065	.077	.114
12 St	1.23	.023	.027	.028	.064	.077	.105
12 ST+C.S.	1.18	.022	.026	.027	.067	.075	.103
C. Spec	1.18	.023	.026	.027	.066	.075	.103
C. Spec+Co	1.18	.023	.026	.026	.066	.076	.102

Table 5: Results for the simultaneous block adjustment (low & high altitude flights)

Different solutions were tried: No self-calibration (no selfcalibr.), 12 BLUH standard additional parameters (12 St), 12 BLUH standard additional parameters with camera specific additional parameters (12 St + C. S.), camera specific additional parameters (C. Spec) and camera specific additional parameters with special additional parameters for solving geometric problems at the image corners that are often seen with digital cameras (parameters 81-88 in BLUH). In all cases the 84 GCPs were used. Table 5 shows an almost 10% improvement in σ_o when self-calibration is applied, however it represents less than a micron. The same trend can be observed in the discrepancies at the GCPs, with little improvement in the planimetric RMSE (X-Y) and a more remarkable improvement in the Z-component.

Block: Low Altitude Flight (GSD=5cm)							
additional parameters	σ_o µm	RMSE 84 GCPs [m]			Maximal Errors 84 GCPs [m]		
		RMX	RMY	RMZ	M-X	M-Y	M-Z
no self calibr	1.15	.022	.025	.028	.050	.078	.072
12 St	1.10	.025	.023	.025	.051	.074	.072
12 St +C. S.	1.05	.020	.023	.024	.058	.073	.074
C. Spec	1.06	.020	.023	.024	.049	.072	.068
C. Spec+Co	1.07	.020	.024	.024	.049	.073	.068

Table 6: Results for low altitude flight (5cm GSD)

This is more noticeable in the high altitude flight and can be explained by the fact that the small systematic errors in plan affect the Z-component by the height-to-base-relation that in the Eagle is approximately 2.93. In any case, the reported accuracies (RMSE, both for the horizontal and vertical components, no self calibration and self-calibration) are below the corresponding GSDs. Nevertheless, one can see from both tables maximum errors that are above the corresponding GSD. For the 5 cm GSD the maximal X/Y differences ranges from 1.74 to 1.85 GSD; whereas for maximal Z differences from 1.36 to 1.44 GSD. As expected, this trend is more significant for the largest GSD (higher altitude flight). Thus the MaxX/Y ranges from 1.86 to 1.97 GSD; whereas for maximal Z differences from 1.94 to 1.98 GSD. The effects of the residual systematic errors are the same being more prominent for higher scale factor (bigger GSD). Nonetheless, in all cases, the maximum is below the threshold of twice the GSD.

Block: High Altitude Flight (GSD=15cm)							
additional parameters	σ_o µm	RMSE 84 GCPs [m]			Maximal Errors 84 GCPs [m]		
		RMX	RMY	RMZ	M-X	M-Y	M-Z
no self calibr.	1.16	.062	.067	.075	.233	.181	.291
12 St	1.14	.059	.064	.070	.214	.175	.293
12 St +C. S.	1.10	.060	.063	.072	.220	.174	.298
C. Spec	1.09	.060	.063	.072	.219	.173	.298
C. Spec+C	1.09	.060	.063	.072	.221	.173	.303

Table 7: Results for high altitude flight (15cm GSD)

Because the primary data capture was performed with automatic matching techniques, there is a large redundancy (in this case more than 36,000) which increases the object point accuracy and in this way the corresponding internal reliability The residuals after applying different sets of additional parameters (self-calibration) are shown in Figure 3.

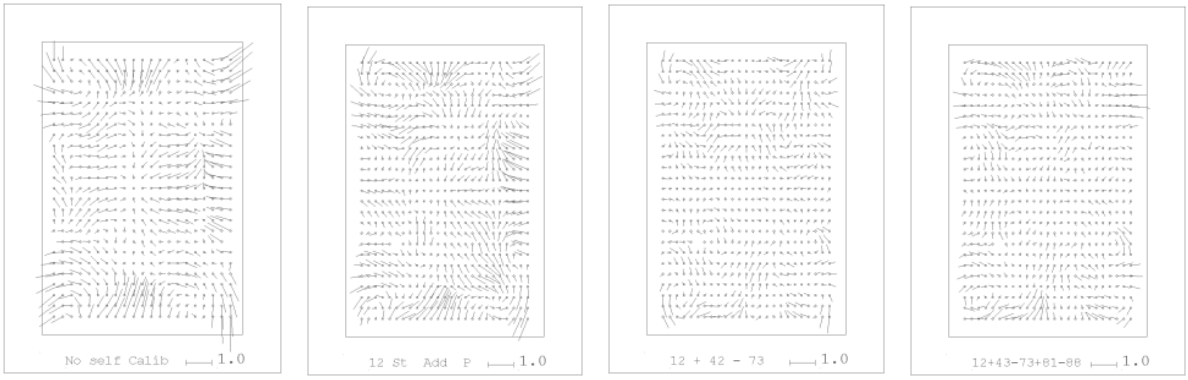

Figure 3: Averaged residuals in image space without self-calibration, with 12 standards additional, 12 standards with camera specific, and 12 standards with camera specific plus 81-88 (corner additional parameters). Vector scale [µm]

We can clearly see that although very small (1 micron or so), after self-calibration with the 12 BLUH standard additional parameters, one can still observe some systematic effects. These practically disappear when we add the camera specific additional parameters to the 12 standard. Practically the same negligible systematic residual pattern remains when the camera specific additional parameters plus the removal of systematic effects in the corners of the camera are used in the adjustment. Here we can observe the cleaning effect of the additional parameters that take care of the corner deformations (81-88), although their use introduces some other very small deformations in other areas of the image (Compare figures 3 above; last two).
By observing figure 4 (below), we can see that it is possible to obtain practically the same magnitude and pattern of systematic residuals after self-calibration using the 12 BLUH standard additional parameters plus the camera specific parameters and the camera specific only. The geometric effects are nearly identical, nevertheless, it is always recommended to use the 12 BLUH standard also (as well as the 81-88) since some of the 12 effects might be present in the images due to external causes (mounting, extreme atmospheric conditions, etc.), as well as systematic deformations in the image corners. This will never constitute an over-parameterization, since the stochastic model used by BLUH automatically removes from the solution those parameters that model systematic effects not present in the images (Passini et. al. ISPRS Istanbul 2004).

Figure 4: Effect of the different sets of Additional Parameters (self-calibration) used in the research

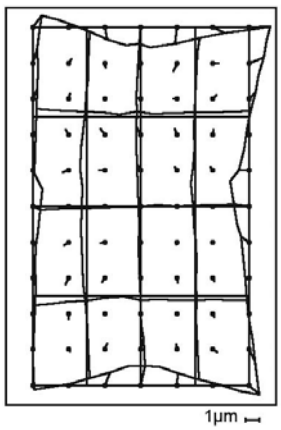

Figure 4a: Parameters 1-12

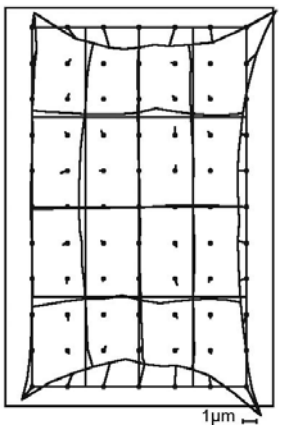

Figure 4b: Parameters 1-12, 42-73

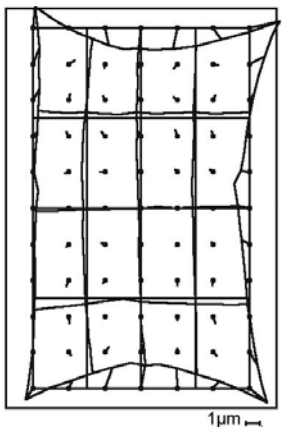

Figure 2c: Parameters 1-12, 42-73, 81-88

In order to determine maximum accuracy achievable with the Eagle, the block was adjusted with a decreasing number of GCPs while using the rest of the 84 as CHKs.

GCPs/ CHKs	ADJ. TYPE	Root mean square differences at check points [m]						
		$\sigma_{0\ \mu m}$	RMX	RMY	RMZ	max X	max Y	max Z
44/ 40	no self calibr.	1.22	.019	.032	.040	.057	.075	.099
	12 St.	1.18	.019	.032	.041	.057	.074	.093
	12 St. + C S	1.13	.019	.032	.040	.058	.076	.089
	C Spec+81-88	1.13	.019	.033	.046	.058	.075	.095
28/ 56	no self calibr.	1.18	.023	.033	-.051	.079	.083	.175
	12 St.	1.14	.024	.033	.044	.086	.081	.170
	12 St. + C S	1.09	.024	.033	.043	.086	.082	.164
	C Spec	1.10	.024	.033	.049	.084	-.082	.158
	C Spec+81-88	1.09	.024	.033	.048	.084	.082	.158
10/ 74	no self calibr.	1.13	.027	.036	.061	.076	.108	.213
	12 St.	1.10	.025	.037	.058	.083	.114	.215
	12 St. + C S	1.02	.025	.036	.058	.083	.114	.219
	C Spec	1.05	.026	.036	.058	.079	.110	.190
	C Spec+81-88	1.06	.026	.037	.058	.078	.111	.179
5/ 79	no self calibr.	1.13	.037	.048	.085	.108	.124	.278
	12 St.	1.09	.037	.046	.071	.111	.129	.261
	12 St. + C S	1.03	.036	.044	.058	.113	.124	.235
	C Spec	1.04	.037	.045	.060	.111	.122	.216
	C Spec+81-88	1.04	.038	.046	.062	.111	.124	.209

Table 8: Absolute accuracy over check points

Analyzing the results from Table 8, we can clearly see that with less GCPs (in general) the discrepancies at check points are larger. This is explained by the fact that (although small) systematic errors are more free to provide their deformation effects; in other words the block (due to the additional effects of the systematic errors) suffers some deformation. This is more noticeable (although once again minimal) in the increase of the values of the RMSE at the CHKs for smaller numbers of GCPs. The largest loss of accuracy (in terms of RMSE-Z over CHKs) is in the Z-components. Although insignificant in terms of absolute differences, the RMSZ raises ~45% (compare 44/40 GCPs-CHKs – no selfcalibration) ; against 5/79 GCPs-CHKs – no self-calibration). This is more noticeable in the maximal Z discrepancies. The maximum drop in accuracy (again insignificant in absolute numbers) is nearly 32.1% (compare 44/40 GCPs-CHKs -12 ST + Camera Specific, against 7/79 GCPs-CHKs – No self-calibration). In other words, with less constraint, the systematic errors are freer to generate their deformation effect

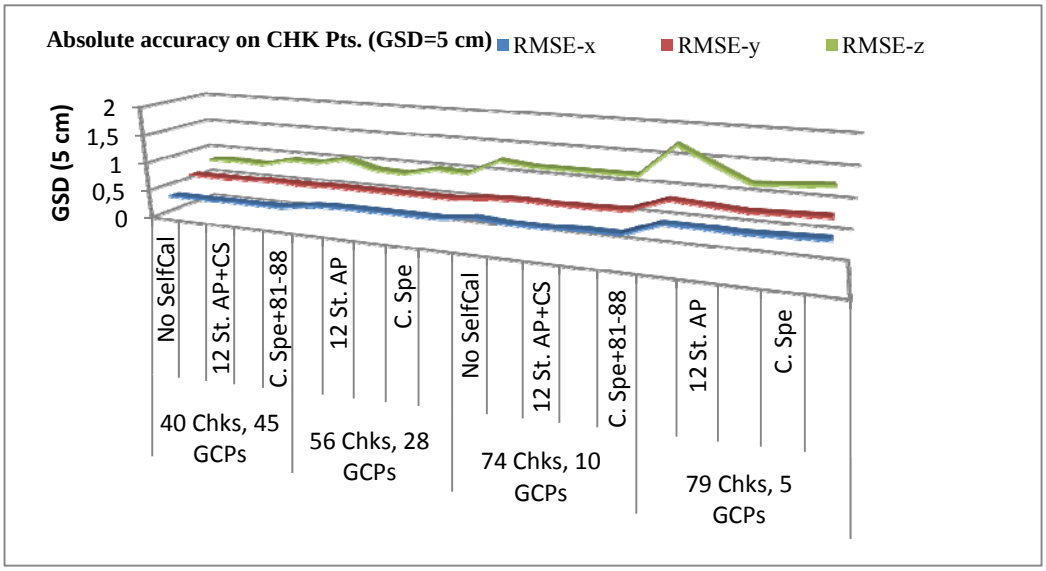

Figure 5: Absolute accuracy (RMSE) at Check Point in terms of GSD (5 cm)

Figure 5 above shows a very stable planimetric accuracy for even lower number of GCPs until the bare minimum is reached (5GCPs) in which case the effect of the systematic errors (more free to spread their effects) provokes a decrease in accuracy but still of sub-pixel magnitude. The effect of the systematic errors on the z-component are less stable for lower number of GCPs and it can reach up to 1.5 GSD value for the bare minimum of GCPs (5 GCPs); a situation practically impossible to be seen in practice life). Nevertheless, in general, the planimetric accuracy in terms of RMSE (for each combination of GCPs and CHKs) becomes better when self-calibration is applied. Additionally, there is no apparent gain or loss in accuracy when additional

parameters that account for the remaining deformations in the corner of the images if the 12 standard parameters. plus the camera specific self-calibration (or in some cases camera specifics only) have been previously applied.

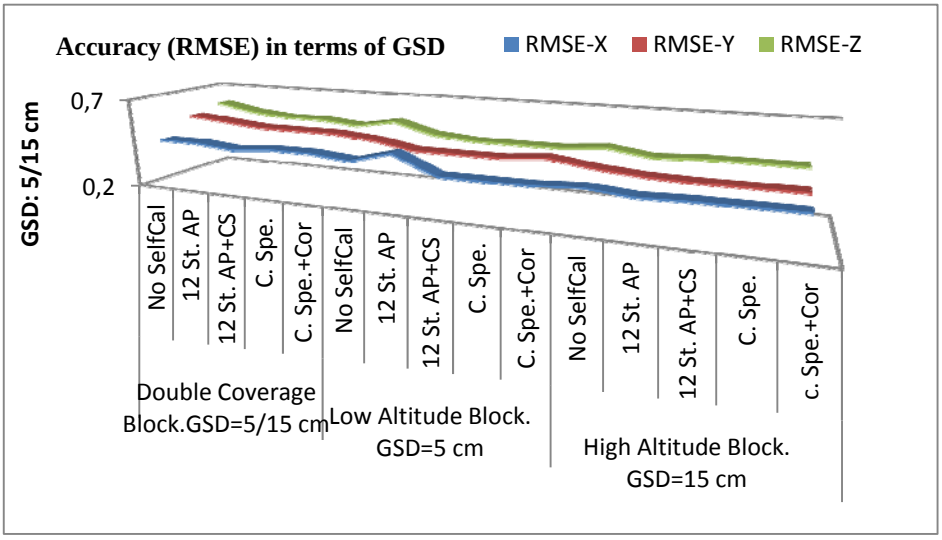

Figure 6: Accuracy (RMSE) on GCPs expressed in GSDs

Figure 6 shows the achieved accuracy in terms of RMSE expressed in GSDs for the 3 studied Block configurations and self-calibration applied sets of additional parameters. From the graph one can see that in no case the RMSE (X, Y or Z) is bigger than the corresponding GSD.
For full GCPs configuration the RMSE (X, Y or Z) remains between 0.4 and 0.6 of the corresponding GSD.

2.3 CAMERA SYSTEM CALIBRATION

For the purpose of carrying out a camera system calibration that would include the corrections to the position of the principal point of the camera, a calibration of the focal length, the misalignment of the camera axis with the IMU axis and a calibration of the distance between the origin of the IMU and the projection center of the camera (also known as the lever arm), a new flight was done over the same study area. All the main geometric parameters of the previous flight were maintained (i.e., GSDs, overlaps, etc.), with the only change being that each strip of the block was flown twice (e.g. forward and reverse direction). This flight pattern allows for the statistically independent determination of the shifts of the airborne GPS positioning and the corrections to the principal point. The used calibration field area meets all the requirements to generate highly precise and reliable system calibration parameters: it is large enough, contains enough highly precise and reliable GCPs, has a strong geometric configuration, it is flown at two different altitudes (5 and 15 cm GSD) and it has each line flown in forward and in reverse directions.
The Calibration field layout is shown in Figure 7 below

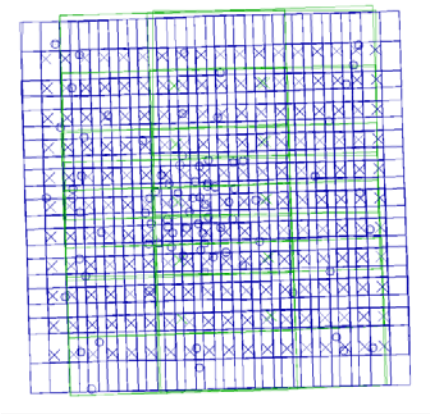

Figure 7. UCE Calibration Field layout. The procedure been followed resulted on the following parameters:

Correction for the focal length	-.008 mm
Shift of principal point in x	.004 mm
Shift of the principal point in y	-.006 mm

Using these parameters for the computation of corrected image points it was then possible to compute the misalignment and GPS shifts as shown below:

```
MISALIGNMENT DETERMINED BY GPSPL

     .00326      .00520      .00065      -.262       .123       .286
     CPITCH       CROLL       CYAW         CX         CY         CZ
                [GRADS]
```

These parameters in turn can be used to correct the orientation provided by the IMU-GPS at every instant of exposure. At this moment we can be in a position to use the camera/system in direct or integrated sensor orientation tasks. In this respect we tried the direct sensor orientation approach by using the corrected orientations (originals provided by the IMU-GPS) and the corrected image coordinates of the used GCPs. In this sense we end-up with two sets, i.e., one observed (Field measured) and the other computed as explained above. A summary of the analysis program shows the achieved results:

```
SQUARE MEAN OF DIFFERENCES
RMSX = +/- 0.029m   RMSY = +/- 0.033m   RMSZ = +/- 0.059m
root mean square differences at 84 GCPs used as check points
MAXIMAL DIFFERENCES
MAX DX =    .071   MAX DY =    .098   MAX DZ =   -.141
```

Using the corrected EOs and the corrected image coordinates we computed the image models with corresponding residual y-parallaxes. The maximum value was found to be: 8.7 microns.

3. THE ZI IMAGING DMCII TEST:

The DMCII 140 and DMCII 250 have been investigated with three different flying heights. The configuration for the DMCII 140 is similar to the configuration of the DMCII 250 shown in figures 8 and 9. The DMCII 230 has been investigated with a test flight at 7cm GSD and an operational block shown in figure 10.

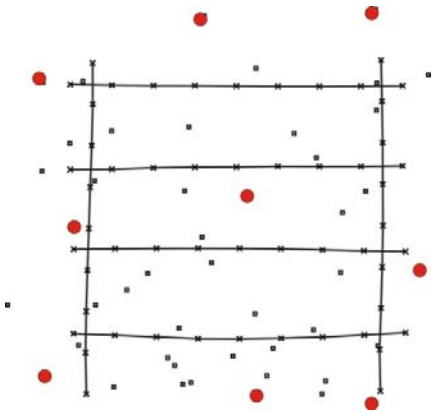

Fig. 8: DMCII 250 block, 5cm GSD

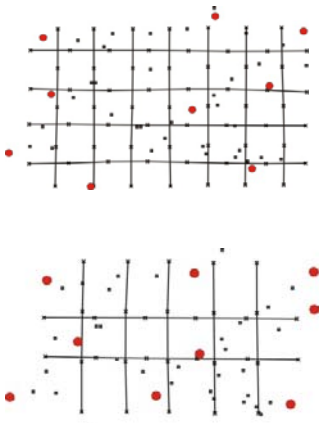

Fig. 9: DMCII 250 block, above 9cm, below 15cm GSD

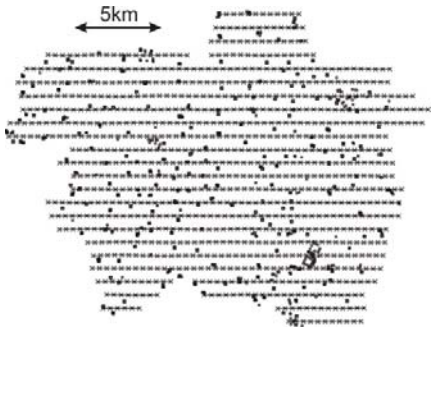

Fig. 10: DMCII 230 block, 7cm GSD

The DMCII-versions are based on a monolithic large size CCD, so the special additional parameters 42-73 are not required. Only the standard parameters 1 – 12 and the special parameters for the image corners 81 – 88 have been tested. All 8 DMCII-blocks did not require the special additional parameters 81 – 88, so for optimal results only the standard parameter 1 – 12 had to be used, which have been reduced by the significance test of the program to in the average 4 used additional parameters.

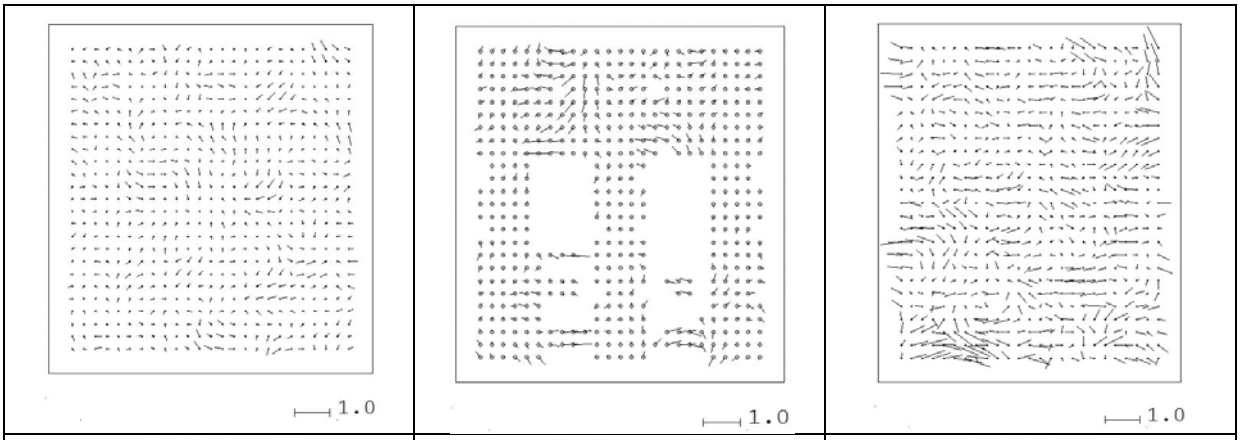

DMCII 140, 9cm GSD	DMCII 230, 7cm GSD	DMCII 250, 9cm GSD

Fig. 11: remaining systematic image errors DMCII

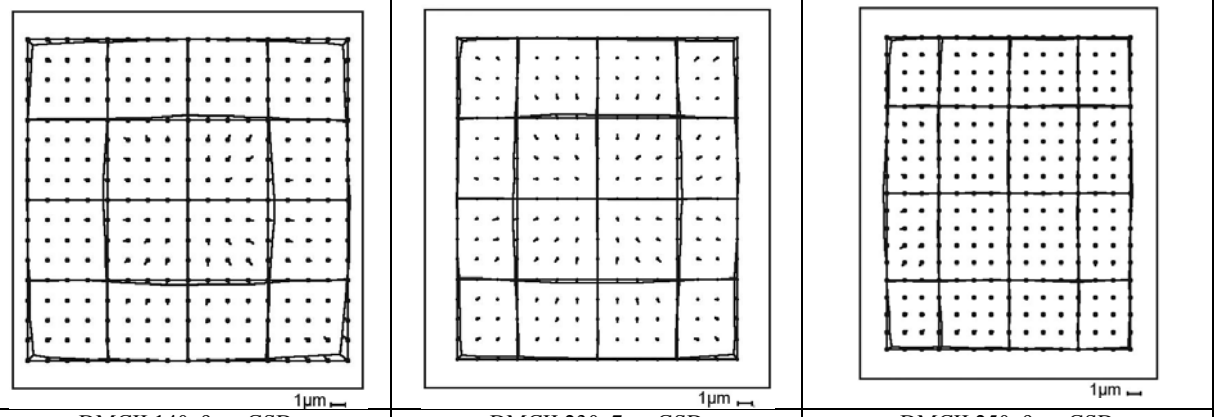

DMCII 140, 9cm GSD	DMCII 230, 7cm GSD	DMCII 250, 9cm GSD

Fig. 12: systematic image errors DMCII

The operational block taken with the DMC 230 with 7cm GSD, for which the systematic image errors are shown in figure 12 and the remaining systematic image errors in figure 11, includes in total 686774 image points or on average 1099 image points per sub-area for which the remaining systematic errors are shown. But the image points are not equally distributed causing gaps in the computation of the remaining systematic image errors. In addition, the vectors above and below the gaps are larger because of the limited number of points in these sub-areas.

In general, the systematic image errors and the remaining systematic image errors are very small. Over all blocks and images the average of the systematic image errors are 0.32µm or 0.06 pixels. The selected results achieved by bundle block adjustment with the DMCII-versions at independent check points shown in figure 10, demonstrate that the bundle block adjustment should be done with self calibration to achieve especially better vertical accuracy, but that the standard set of 12 additional parameters is sufficient. All these blocks are based on 8 to 9 GCPs with the exception of the very large operational block requiring more GCPs. The not shown results are corresponding to this. Of course a block with crossing flight lines results in better accuracy; by this reason the results based on reduced coverage (double and single blocks) are also shown. Even with single blocks the results achieved at check points are also in the more critical height component below 1 GSD in spite of the base to height relation of base to height relation of 1:2.8 up to 1:3.4. The blocks with all images (always left hand bar group) have the GCPs in the average in 8.4 / 6.2 respectively 9.6 images and the check points in 10.6 / 6.2 respectively in 12.7 images. Based on this the vertical accuracy at the check points is in the range of 0.6 GSD.

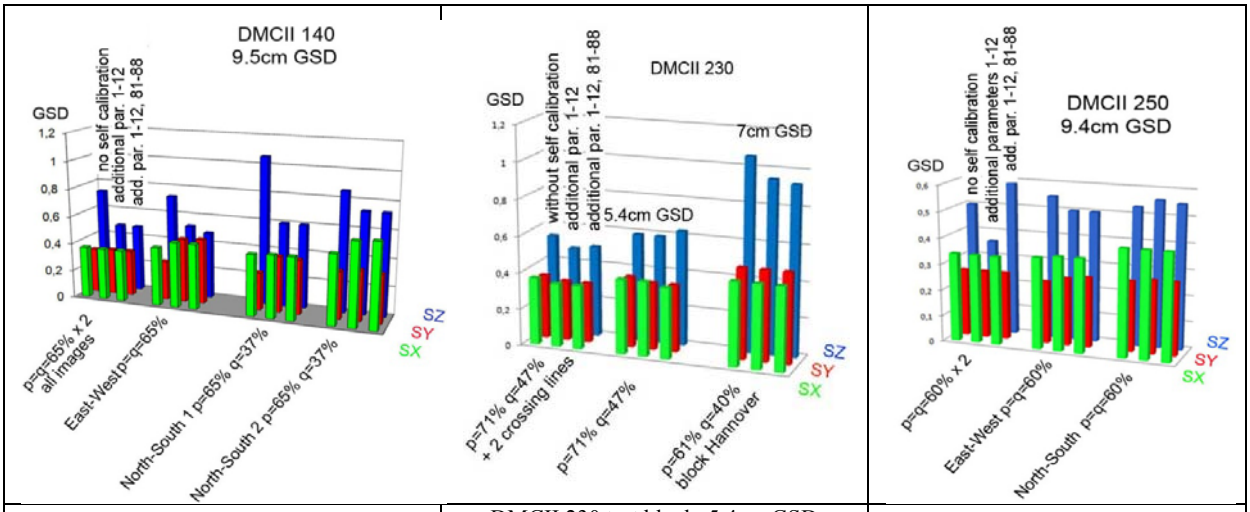

DMCII 140 test block, 9cm GSD	DMCII 230 test block, 5.4cm GSD + operational block, 7cm GSD	DMCII 250 block, 9cm GSD

Fig.11: Accuracies achieved with DMCII-blocks at independent check points, p=end lap, q=side lap

4. RADIOMETRIC IMAGE QUALITY

The radiometric image quality can be determined by edge analysis. A sudden change of the gray values in object space is causing a continuous change of the gray values in a profile perpendicular to the edge. If this gray value profile is differentiated, it leads to the point spread function. The width of the point spread function leads to the factor for effective resolution (Jacobsen 2008). This factor multiplied with the pixel size or the GSD leads to the effective resolution which is important for the identification of objects. By simple theory this factor should not be below 1.0, but by image enhancement this can be, but it is causing a higher signal to noise relation.

camera	blue, pan-sharpened	green, pan-sharpened	red, pan-sharpened
DMCII 230	0.98	0.97	0.98
DMCII 250	0.87	0.88	0.84
UltraCam Eagle (UCE)	1.01	1.02	1.03

Tab. 9: Factor for effective pixel size determined by edge analysis

The small differences of the factor for effective resolution of the three pan-sharpened spectral bands are caused by the fact, that the geometric resolution is dominated by the higher resolution panchromatic band. In general no loss of information can be seen at the factors for effective resolution in table 9, but it is obvious at the images, that they have been edge enhanced. The enhancement enlarges the image noise. The noise at homogenous areas for the UCE is in the range of 4 to 5 grey values, while it is in the range of 2 for the DMCII-versions. The slightly higher value of the effective pixel size for the UCE is due to the smaller pixel value and smaller dimension of aperture.

7. CONCLUSION

It is important to emphasize once more that this is not a comparison study between the two types of cameras. The conducted flights were carried out in different places and times of the year/latitude of the place, hence different illumination of the terrain. The geometric parameters of the flights are totally different (including the UCE flights are of double coverage). The number, distribution and characteristics of the GCPs are different. The GSD is different for each camera. In view of all above, the authors have summarized the obtained results of each test. Nevertheless we can summarize our findings for each studied camera:

7.1. UltraCam Eagle

1. Under the Geometric parameters of the Flights been used in the present investigation, the reduction of the number and distribution of GCPs does not aggressively affects the overall accuracy of the Blocks. The rate of change of the standard deviation is practically negligible.
2. Nevertheless, with less control discrepancies starts to show up especially in the vertical component. The changes in the horizontal components are insignificant leaving the block more stable.
3. Although not unusually large, those discrepancies denounce the presence of systematic errors. These have been respected and removed using self-calibration approach.
4. The additional parameters been used are the 12 standard included in program system BLUH, the camera specific and eight especially derived additional parameters for solving geometric problems at the image corners, often seen with digital cameras.
5. From the results we can see that it is possible to obtain practically the same magnitude and pattern of systematic residuals after self-calibration using the 12 BLUH standard additional parameters plus the camera specific parameters and the camera specific only. The geometric effects are nearly identical, nevertheless, it is always recommended to use the 12 BLUH standard parameters also (as well as parameters 81-88) since some of the 12 effects might be present in the images due to external causes (mounting, extreme atmospheric conditions, etc.), as well as systematic deformations in the image corners. This will never constitute an over-parameterization, since the stochastic model used by BLUH automatically removes from the solution those parameters that model systematic effects not present in the images (Passini et. al. ISPRS Istanbul 2004).
6. In general, the loss in accuracy (in terms of RMSE) caused by the systematic errors is limited for the used block configuration with 60% side lap and crossing flight lines.
7. A boresight calibration with each strip in a forward and reverse pattern allows the precise determination of the correction to the position of the principal point of the camera eliminating the high correlation that exists between the GPS shift and this important point. If the flight takes place at two different altitudes, it is also possible to calibrate the focal length of the camera. Misalignment between camera and IMU axis and shifts of the system (IMU-airborne GPS) and the projection center it is also possible. Results are shown above.
8. The system calibration parameters allows the correction of the image orientations been observed (IMU-airborne GPS) during flight and the corrections to the position of the principal point of the camera can be applied to all observed point of the images. Using corrected image coordinates of the GCPs, the corrected image orientations captured during flight and the new calibrated focal length a new set of coordinates of GCPs were computed. When compared with the field observed coordinates RMS in the range of 4 cm and 6 cm for plan and height respectively with maximum discrepancies in the order of 9 cm and 14 cm respectively. Moreover, the practiced direct sensor orientation preserved the high internal stability of the block since the largest vertical parallax found was 8.7 microns.
9. The computed factors for effective resolutions are only slightly bigger than one meaning that there is no remarkable loss of information or in other words the real GSD is nearly equal to the nominal GSD. Nevertheless, this is the result of an image enhancement leading to some image noise. This did not cause problems for matching .

7.2.DMC II

The analyzed data sets show very small systematic image errors, smaller as for any other photogrammetric camera. The size of systematic image errors can be ignored for data acquisition in models. For all data sets, even the single blocks with approximately 60% end lap and 40% side lap, the root mean square differences at the critical height component is below 1 GSD. The effective ground resolution corresponds to the nominal ground resolution and the image noise is limited.

REFERENCES

Jacobsen, K. (2011): Geometric Property of Large Format Digital Camera DMC II 140. In: PFG 2011 / 2, pp. 071 – 079, March 2011

Passini, R.; Jacobsen, K. (2009): Accuracy and radiometric study on very high resolution digital camera images, ISPRS Hannover Workshop 2009

Passini, R.; Jacobsen, K. (2008): Geometric Analysis on Digital Photogrammetric Cameras: ASPRS 2008 Annual Convention. Portland, 2008, 11 S

Passini, R.; Jacobsen, K. (2008): Accuracy analysis of large size digital aerial cameras: IntArchPhRS. issue XXXVII, part B1. Peking, 2008, S. 507-514

Jacobsen, K. (2008): Geometrisches Potential und Informationsgehalt von großformatigen digitalen Luftbildkameras. In: PFG (2008), Nr. 5, S. 325-336

Passini R.; Jewell D.; Jacobsen K. (2002): An Accuracy Study on a large Airborne GPS Aero Triangulation Block, ASPRS Annual Convention, Washington, 2002, 13 S.,